25 kW Low-Temperature Stirling Engine for Heat Recovery, Solar, and Biomass Applications

Lee SMITH[a], Brian NUEL[a], Samuel P WEAVER[a,*], Stefan BERKOWER[a], Samuel C WEAVER[b], Bill GROSS[c]

[a]Cool Energy, Inc, 5541 Central Avenue, Boulder CO 80301
[b]Proton Power, Inc, 487 Sam Rayburn Parkway, Lenoir City TN 37771
[c]Idealab, 130 W. Union St, Pasadena CA 91103

*Corresponding author: spweaver@coolenrgy.com

Keywords: Stirling engine, waste heat recovery, concentrating solar power, biomass power generation, low-temperature power generation, distributed generation

ABSTRACT

This paper covers the design, performance optimization, build, and test of a 25 kW Stirling engine that has demonstrated > 60% of the Carnot limit for thermal to electrical conversion efficiency at test conditions of 329 °C hot side temperature and 19 °C rejection temperature. These results were enabled by an engine design and construction that has minimal pressure drop in the gas flow path, thermal conduction losses that are limited by design, and which employs a novel rotary drive mechanism. Features of this engine design include high-surface-area heat exchangers, nitrogen as the working fluid, a single-acting alpha configuration, and a design target for operation between 150 °C and 400 °C.

1. INTRODUCTION

Since 2006, Cool Energy, Inc. (CEI) has designed, fabricated, and tested five generations of low-temperature (150 °C to 400 °C) Stirling engines that drive internally integrated electric alternators. The fifth generation of engine built by Cool Energy is rated at 25 kW of electrical power output, and is trade-named the ThermoHeart® Engine. Sources of low-to-medium temperature thermal energy, such as internal combustion engine exhaust, industrial waste heat, flared gas, and small-scale solar heat, have relatively few methods available for conversion into more valuable electrical energy, and the thermal energy is usually wasted. Specifically targeted to be powered by such heat sources, the ThermoHeart Engine has received widespread technical and commercial interest, especially in applications producing less than 100 kW_e, where current power conversion technologies suffers performance challenges and often economic infeasibility. By demonstrating a working Stirling engine generating electricity at conversion efficiencies significantly greater than those attained by existing technologies, CEI has created the opportunity to produce cost-effective, emissions-free electric power from these low-to-medium temperature heat sources.

To date, the prototype model of the 25 kW 5th generation engine has demonstrated 31.0% thermal-to-electrical conversion efficiency at 329 °C hot-side and 19 °C cold-side temperatures. The Carnot limit for these temperatures is 51.5%, and the resulting fraction of the Carnot limit demonstrated is 60.2%. The 25 kW_e output power rating is the maximum electrical power that the engine would produce at the standard rating conditions of 400 °C hot-side and 20 °C ambient temperatures, and also at a ratio of any hot-side to cold-side absolute temperatures of the heat transfer fluids that is about 2.26. Some design details were shared at the 2015 Geothermal Technologies Office peer review poster session, but this is the first widespread technical discussion of this engine layout and detailed testing results.

The Stirling thermodynamic cycle has several advantages over competing approaches typically used in low-to-medium temperature heat source applications: thermal-to-electrical conversion efficiency is excellent, medium-scale opportunities can be addressed (10 kW to 200 kW), part-load performance is very good, proper operation of the thermodynamic cycle is not sensitive to either hot- or cold-side temperatures, and Stirling engines do not contain environmentally hazardous gases or fluids. Restricting the hot-side temperature to between 150 °C and 400 °C enables several novel approaches to be incorporated into the 25 kW ThermoHeart Engine, such as self-lubricating, low-wear-rate bearing surfaces, the option of metallic or non-metallic regenerators, high-effectiveness, low-cost shell-and-tube heat exchangers, and a unique linear-to-rotary mechanism to transfer mechanical work from the pistons to the built-in electric alternator.

A 25 kW ThermoHeart Engine equipped with a non-metallic film regenerator (not in the current operating prototype) and optimized for low-temperature applications is estimated to be able to produce 20 kW_e at hot-side and ambient temperatures of 200 °C and -6 °C, respectively. Sites that have low ambient temperatures enable full power to be generated with hot-side temperatures less than the maximum limit, which will influence how the heat source or the engine's charge pressure is managed. The control system can also limit power output to 25 kW_e (or less) by controlling engine speed to be under the 600 rpm maximum design speed.

1. MATERIAL AND METHODS

The following key components and processes are described, along with methods used in their investigation, design, fabrication, and troubleshooting:

- Working fluid
- Heat exchangers
- Regenerator
- Linear-to-rotary mechanism
- Further objectives and accomplishments

Working fluid: An early design decision was made to compare the use of nitrogen as a working fluid to the more common selection of helium or hydrogen. Hydrogen embrittles some metals, is hard to seal, and is potentially explosive. Helium is relatively expensive, depleting as a resource, and relatively hard to seal as well. One of the losses in the actual thermodynamic process occurs when the working fluid leaves a heat exchanger at one temperature and mixes with the working fluid between the heat exchanger and its corresponding piston at a different temperature. This loss is exacerbated with a monoatomic gas such as helium [1], [2]. At the same temperature and pressure, nitrogen is denser than hydrogen or helium, and thus has a lower leakage rate through certain piston sealing structures. Early simulations showed that nitrogen is quite feasible as a working fluid, but to achieve conversion efficiencies as high as helium or hydrogen requires that the heat exchangers and regenerator accommodate the lower thermal conductivity of nitrogen. This is done by increasing the surface area of their heat transfer surfaces. Accurate models developed by NIST of the thermodynamic [3] and transport [4] properties of nitrogen were incorporated into CEI's proprietary engine design software tool, enabling engine and refrigerator designs with cold-side temperatures extending down to the cryonic range to be analyzed.

Heat exchangers: An examination of Stirling engine applications has shown that, historically, integrated hot heat exchangers, which act also as an engine pressure vessel, have been a recurring point of failure, requiring reconditioning of the engine to remedy. An early design decision was made to deliver thermal energy into the CEI engines via a heat transfer fluid which circulates between an external, atmospheric pressure hot heat exchanger and the internal engine heat exchangers which bear the full working fluid charge pressure. In the case of failure of the external heat exchanger, that component can be replaced or re-conditioned without requiring the pressure vessel of the engine to be opened.

The first and most significant step toward achieving mass-producible heat exchangers was choosing a shell-and-tube configuration, instead of continuing with the plate-fin configuration of Cool Energy's previous designs. Although the shell-and-tube configuration has more parts (because of the large number of tubes), it has fewer different parts than does the plate-fin configuration. It is anticipated that in volume production the tubes, which are cut from standard, inexpensive tubing, would be inserted into the tube sheets robotically, though for the prototyping phase these heat exchangers were assembled by hand. For the prototype, off-the-shelf perforated sheet, with holes of a diameter close to that of the tubes, was cut into large disks to become tube sheets. These, along with the tubes, were assembled into supporting castings that function as the shell of the shell-and-tube configuration, and vacuum-brazed.

The heat exchangers in the 25 kW prototype engine each have 8100 tubes, and produce very high-effectiveness heat transfer between the heat transfer fluid on the shell side and the nitrogen gas working fluid on the tube side. Future versions will employ custom-punched tube sheets rather than off-the-shelf tube sheets, which will eliminate the need for an edge ring component currently used to help plug un-needed holes at the perimeter. Each heat exchanger is leak-tested after brazing, finish-machined, and then hydrostatically pressure tested at 6.2

MPa before being placed in service. Figure 1 shows the CAD model and the as-built hardware for the hot heat exchanger. Figure 2 shows the same for the cold heat exchanger.

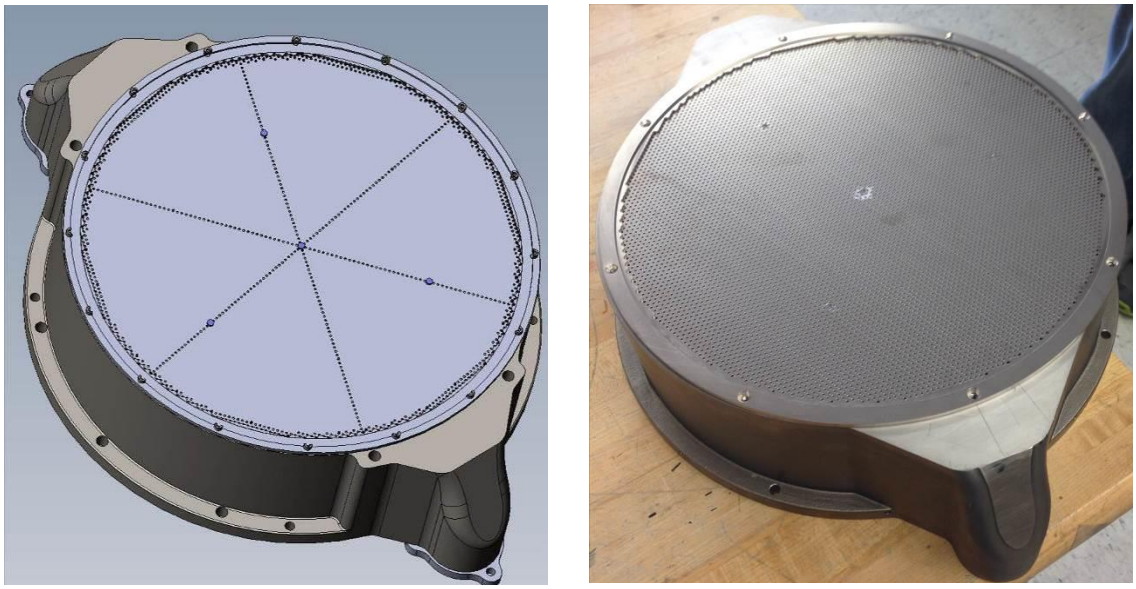

Figure 1. CAD design (left) and as-built hardware (right) of the hot heat exchanger.

The plate-fin heat exchangers in Cool Energy's previous two engine designs had an appreciable temperature difference between the gas and liquid streams. This temperature drop occurred in part from the high heat flux having to conduct edgewise through both the gas side and the liquid side fins, and through thick plates to which the fins were brazed separating the gas and liquid phases. These plates are required to be substantially thick in order to withstand the high pressure on the gas side, as the pressure on the liquid side is near atmospheric pressure. This substantial thickness imposes significant temperature drop. The shell-and-tube concept inherently does not have the extra temperature drops caused by the fins and plates.

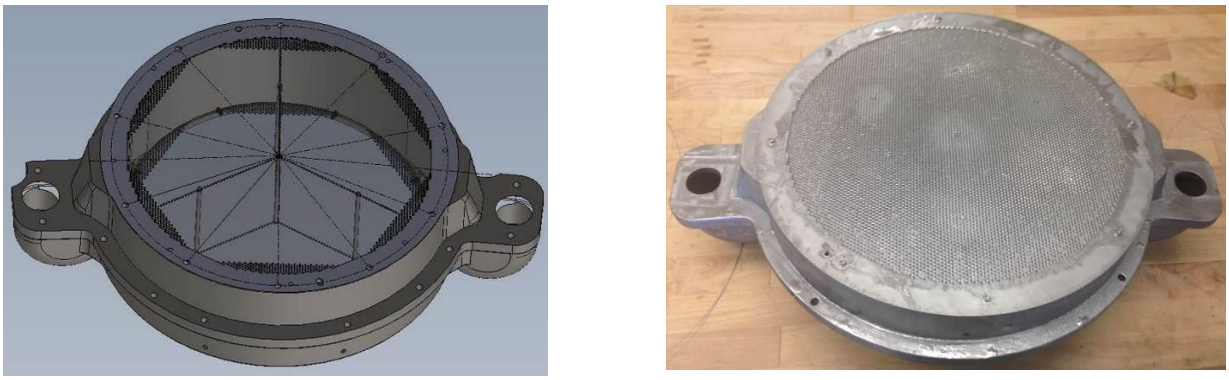

Figure 2. CAD design (left) and as-built hardware (right) of the cold heat exchanger.

Because the tubes are structurally more efficient to withstand internal pressure than the plates, and are of small diameter and hence need only thin walls to withstand the gas pressure, the tubes do not take up as much usable interior volume as do the fins and plates. The heat exchanger design for the 25 kW engines loses less than 10% of the interior volume to the tube walls, compared to 50% lost to the fins and plates in the previous design. This advantage allows greater flexibility in future optimization of the heat exchangers, to be directed toward further cost reduction while maintaining thermal performance.

Sensitivity studies of the heat exchanger tube count versus engine performance have resulted in plans for future heat exchangers to have 5500 tubes rather than the current 8100, improving manufacturability while reducing material cost and assembly time.

Regenerator: During the development of the previous 4 engine generations, CEI has tested many distinct options for regenerator material and construction. For applications below 315 °C, a non-metallic film can be utilized. After discussing manufacturing processes of the non-metallic regenerator with multiple manufacturers, it became clear that the production volume needed to implement this type of process at a supplier facility would need to be much higher than the amount of material needed for prototypes. Two potential suppliers of an alternative regenerator material, woven stainless steel screen, were found when evaluating options.

Table 1. Comparison of three regenerator types. Maximum hot-side temperature for the non-metallic regenerator is limited to 300 °C. Cold-side temperature is 25 °C.

	Hot-Side Temp, °C	Heat In, W	Heat Rejected, W	Gross Electric Power, W	Gross Thermal to Electrical Efficiency
Non-metallic film mid temp	300	94250	69002	25368	26.9%
	250	89596	68981	20739	23.1%
	200	84466	69069	15526	18.4%
	150	78640	69252	9521	12.1%
Metallic screen	350	89406	63989	25548	28.5%
	300	84676	62765	22048	26.0%
	250	79608	61616	18136	22.7%
	200	74089	60507	13731	18.5%
	150	68011	59436	8729	12.8%
Metallic foil	350	87311	61445	25996	29.7%
	300	82871	60558	22450	27.1%
	250	78152	59816	18480	23.6%
	200	73099	59244	14004	19.1%
	150	67577	58820	8912	13.2%

These two suppliers could also laser-cut the screen into disks, which when stacked into many layers form an effective regenerator. The laser-cutting operation is critical for two reasons—dimensional accuracy, and edge stability. The regenerator material (of either design) is inserted into titanium cylinders, titanium being chosen for its strength and low thermal conductivity and thus its ability to reduce thermal conduction losses from the hot heat exchanger to the cold heat exchanger. Because excessive clearance between the screen edges and the cylinder wall would allow gas to bypass the disks, thus reducing the regenerator's effectiveness, the high accuracy of laser-cutting allows this clearance to be small. Laser-cutting also welds the wires together along the edge of the disk, thus stabilizing the edge. Punching, a typical mechanical technique for making screen discs, not only has lower accuracy and thus requires the clearance to be large, but also leaves many short wires near the

edge held in place by only friction or the weak interlock between wires bent in the weave. It is CEI's experience that small fragments of wire are shed from such edges and driven into the heat exchangers and eventually into the engine cylinders by the rapid working fluid flow. Metal fragments in the engine cylinders cause high friction between the pistons and cylinders, scratch the cylinder walls, pistons, and piston rings, and degrade engine performance and lifetime.

The laser-cut, woven stainless steel screen regenerator, which allows for both low-temperature and medium-temperature operation, was found through simulation to perform well enough at the low temperatures expected in the low-temperature application to achieve engine efficiencies extremely close to those obtainable with the non-metallic regenerator. Table 1 above shows the predicted performance of the original non-metallic and the screen regenerators, along with the predicted performance of a metallic foil regenerator [5], [6]. It is expected that the metallic foil regenerator, which has better efficiency, will also be easier to manufacture. Although the power output was modeled to be slightly lower with the screen regenerator, the thermal performance of the screen regenerator is more than sufficient to validate the operation of the engine across its whole temperature range. In addition, the power output of the engine with a screen regenerator can be made nearly equal to that with a non-metallic regenerator by changing engine speed or charge pressure.

Figure 3 shows the CAD model and the as-built hardware of the screen regenerator in its shipping container. Figure 4 shows the CAD model and the as-built hardware of a fully assembled heat exchanger stack, consisting of, from bottom to top, a cold diffuser, cold heat exchanger, regenerator, hot heat exchanger, and hot diffuser.

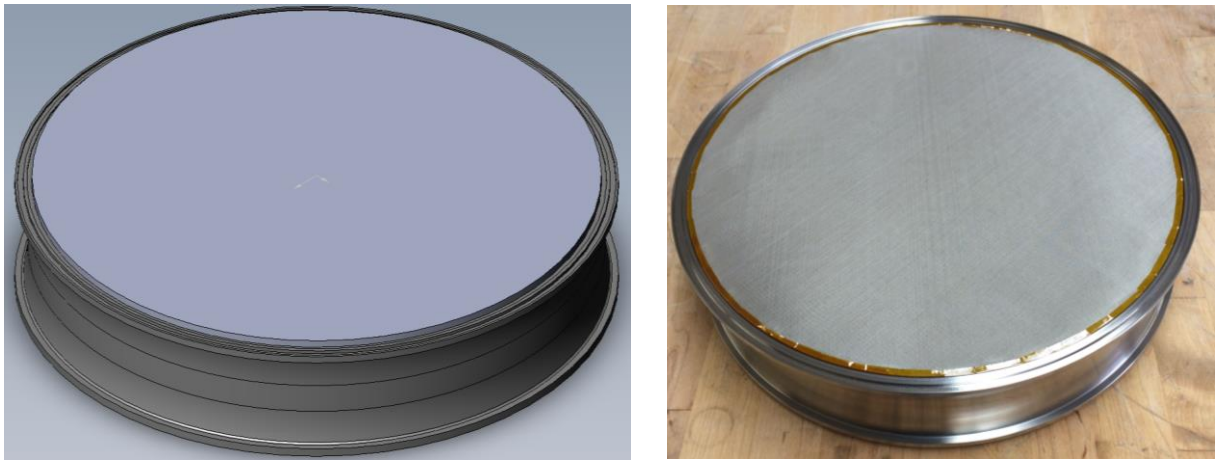

Figure 3. CAD design (left) and as-built hardware (right) of the stacked screen regenerator.

Figure 5 shows the four completed heat exchanger stacks assembled onto the cold plate, the main mounting surface for much of the rest of the engine. The cold plate also delivers the cold-side fluid to the cold heat exchangers through embedded channels in the plate.

Linear-to-rotary mechanism

Mechanism Design: The linear-to-rotary mechanism performs two functions: 1) produce the correct thermodynamic phase relationship between the hot-side and cold-side pistons; and

2) transform the force generated on the pistons into torque on a shaft to drive a rotary permanent magnet alternator.

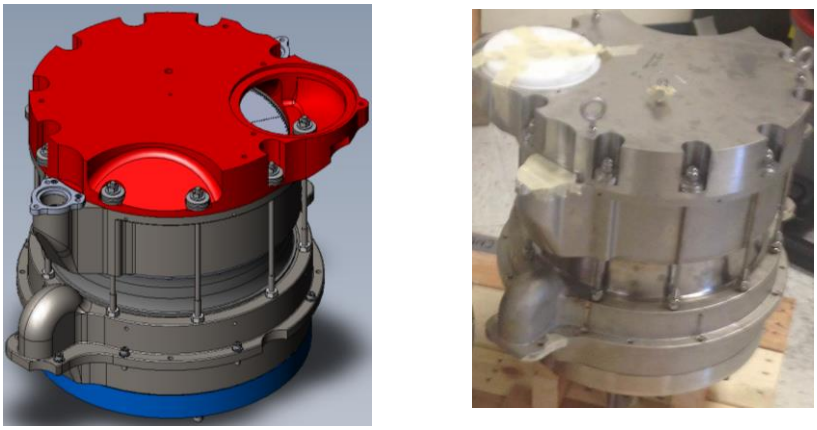

Figure 4. CAD design (left) and as-built hardware (right) of a full heat exchanger stack.

Figure 5. Four thermodynamic circuits fully assembled onto the cold plate.

As CEI has developed its engines, it has settled on the single-acting alpha configuration as having the highest potential for performance and reliability at low to medium hot-side temperatures. When scaling up to the 25 kW_e engine, it became clear through design costing studies that at larger sizes, a rotary mechanism, as opposed to a slider-crank mechanism, would have lower costs, due to minimizing the diameter of the external pressure vessel, and lower thermal conduction and convection losses, due to minimizing the area of contact between the hot-side and cold-side regions. As a result of further study, it was conceived that by having four thermodynamic circuits arranged around the rotary mechanism, the hot piston of one thermodynamic circuit and the cold piston from an adjacent thermodynamic circuit could be attached to a single actuator, and the set of four actuators attached to a single cam and cam-follower mechanism, reducing cost, mass, and size significantly. The connection from the mechanism to each cold piston is by a simple rod, and to each hot piston by a rigid assembly called a "bail." Figure 7 shows three notional thermo-mechanical variants of this "rotary-bail" configuration having four thermodynamic circuits:

Thermal offset configuration (left): The hot piston of one thermodynamic circuit and the cold piston of an adjacent thermodynamic circuit are coaxial on the same actuator, but the hot and cold pistons of the same thermodynamic circuit are offset (not coaxial).

Mechanical offset configuration (center): The hot piston of one thermodynamic circuit and the cold piston of an adjacent thermodynamic circuit are offset (not coaxial) on the same actuator, but the hot and cold pistons of the same thermodynamic circuit are coaxial.

Hybrid offset configuration (right): The hot piston of one thermodynamic circuit and the cold piston of an adjacent thermodynamic circuit are offset (not coaxial) on the same actuator, and the hot and cold pistons of the same thermodynamic circuit are also offset (not coaxial).

Each of the three variants described above can be implemented on either of two linear-to-rotary mechanisms for coupling the linear motion of the pistons to the rotary motion of the axle: A barrel-cam with rail-supported crosshead carriages, or a cam and cam followers with crosshead motion synthesized by Watt linkages. All three thermo-mechanical variants shown in Figure 6 are coupled with a barrel-cam mechanism. Figure 7 shows the two variants of the linear-to-rotary mechanism.

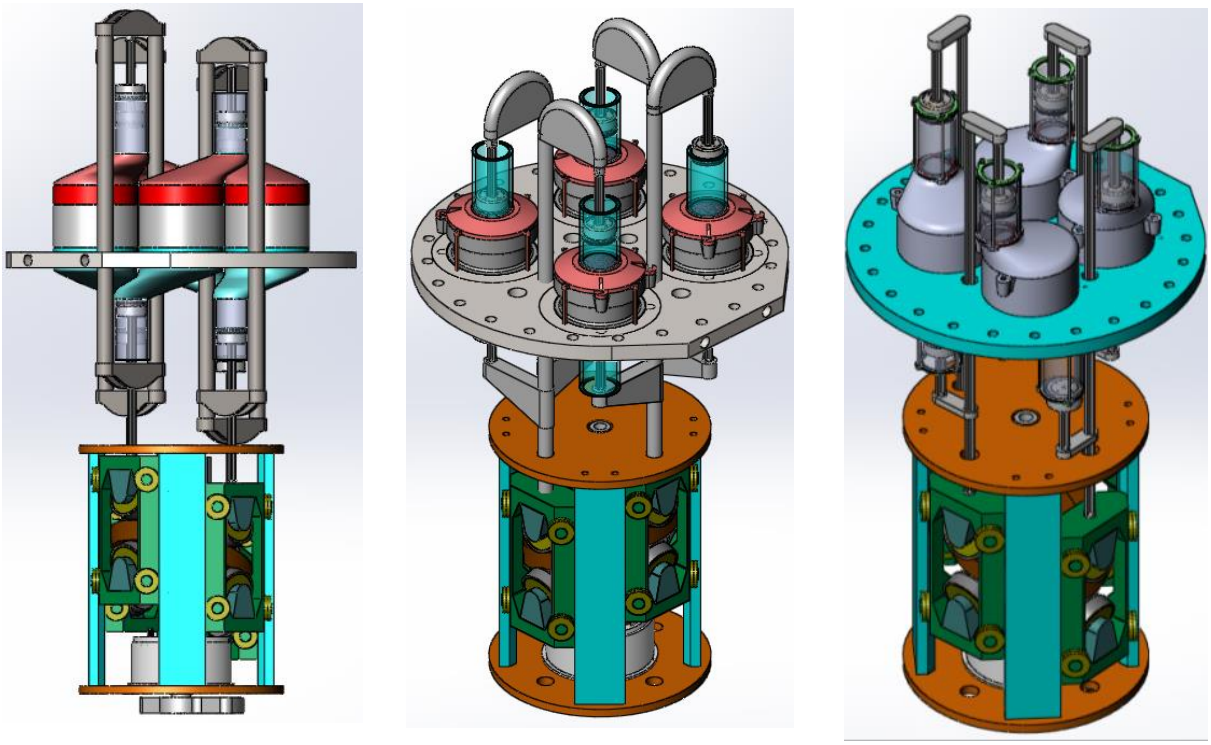

Figure 6. Three examples of the rotary-bail configuration. Full thermal offset configuration (left); full mechanical offset configuration (center); hybrid offset configuration (right).

The Watt linkage is a four-bar linkage that synthesizes a highly accurate, nearly straight line motion at a special point, called the "linear-motion" point, on its center link over a limited distance. This point can be used as a crosshead, where the end of a cold piston rod or a hot piston bail opposite its respective piston may be attached with a pivot. Even though the motion of the Watt linkage is planar, its structure is able to absorb forces in all directions except those in the direction of motion of the linear-motion point. These forces transform into

torque on the main axle. The slight imperfection in the straightness of motion of the linear-motion point results in only small side loads being imposed between the pistons and cylinders.

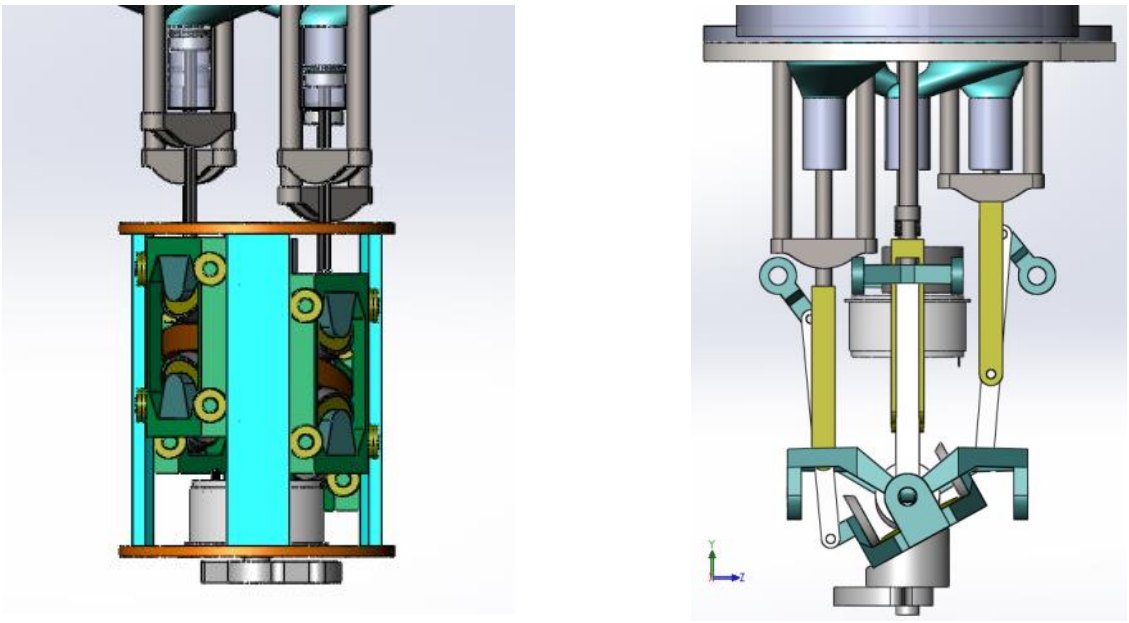

Figure 7. Barrel-cam with rail-supported crosshead carriages (left); cam and cam followers with crosshead motion synthesized by Watt linkages (right).

In the cam and cam-followers mechanism, with crosshead motion synthesized by Watt linkages, the cam and each cam follower are cones whose apexes are coincident. Thus, there is no skidding at the contact interface between the cam and each cam follower, as the motion is that of one cone rolling around another. This relationship is shown in Figure 8. In the barrel-cam mechanism, however, there is inherent skidding at the contact interface between the cam and the cam followers, which in mechanisms sized for the 25 kW ThermoHeart Engine can be reduced to less than 0.5% of the rolling distance, but cannot be eliminated.

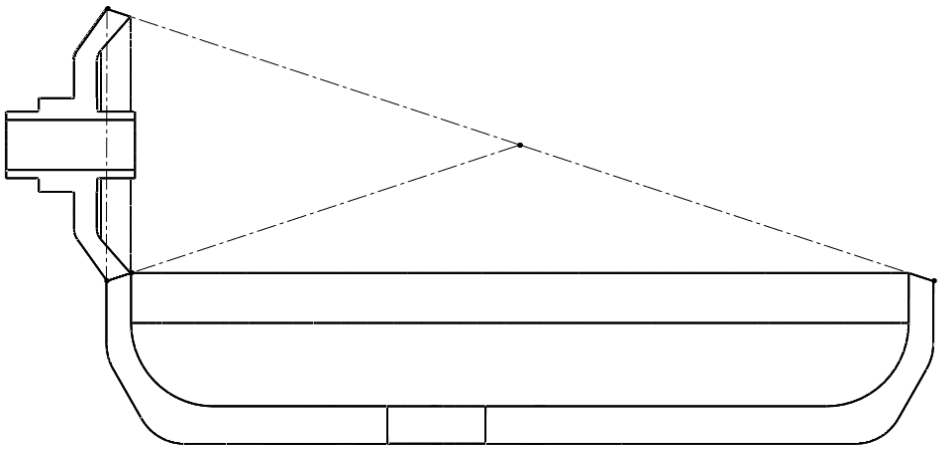

Figure 8. Apex of the conical surface of the cam follower (small diameter wheel) shown coincident with the apex of the conical surface of the cam (large diameter wheel).

The axis of the cone of the cam is inclined with respect to the axis of rotation of the main axle. The apexes of the cones of the cam and each cam follower lie on the axis of rotation of the main axle. Each cam follower is mounted to the input link of a Watt linkage. The axis of rotation of the input link's grounded end intersects and is perpendicular to the axis of rotation of the main axle, and also intersects the apexes of the cones of the cam and cam follower. As the main axle rotates the cam, the cam follower and input link together swing in an arc.

After trading off the risks and benefits of the six combinations of the variants, CEI down-selected the hybrid offset configuration and the cam and cam followers with crosshead motion synthesized by Watt linkages. In this combination, the cylinders are not too far offset from the centers of the heat exchangers, so the diffusers connecting the cylinders to the heat exchangers add only a relatively small amount of dead volume, and the high mechanical efficiency of a mechanism that has no inherent skidding at any of the rolling interfaces is retained. Figure 9 shows the CAD design and the as-built engine mechanism.

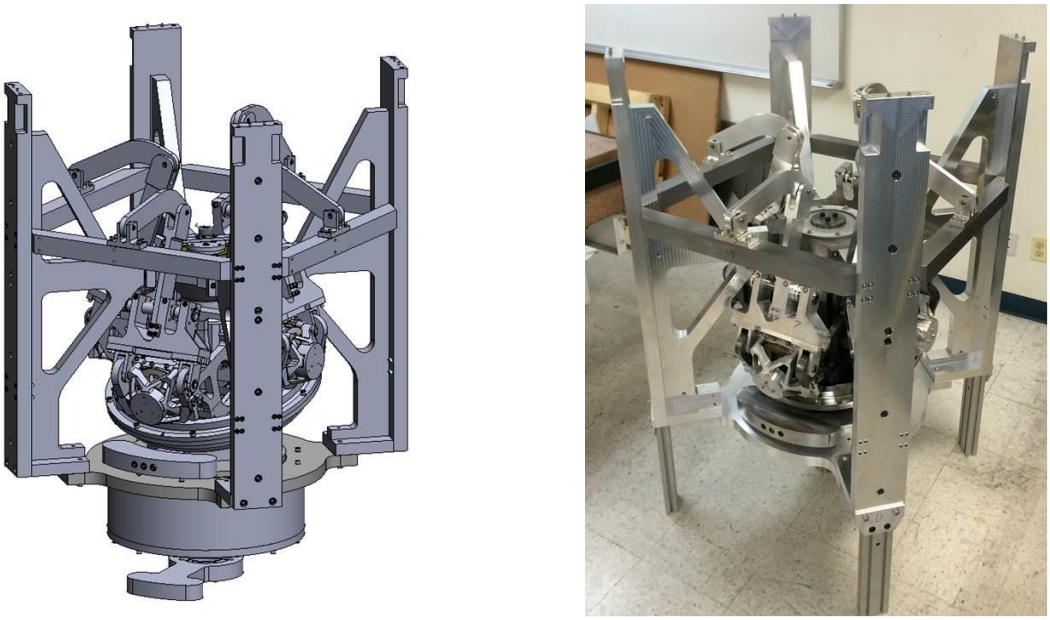

Figure 9. CAD design (left); as-built engine mechanism (right).

Further objectives and accomplishments

Pressure vessel: A cost model of the pressure vessel was developed and incorporated into the Stirling engine analysis program, to help identify optimum engine designs as influenced by the pressure vessel cost. The pressure vessel, designed to ASME code, includes feedthroughs for the hot heat transfer fluid that support thermal barrier fittings, to reduce heat conduction to the pressure vessel wall. To accommodate thermal expansion, flexible distribution piping connects the thermal barrier fittings to the hot heat exchangers.

The cold plate is sandwiched between the flanges of the pressure vessel. The relationship between the internal assembly, mounted entirely onto the cold plate, and the pressure vessel is shown in Figure 10 below.

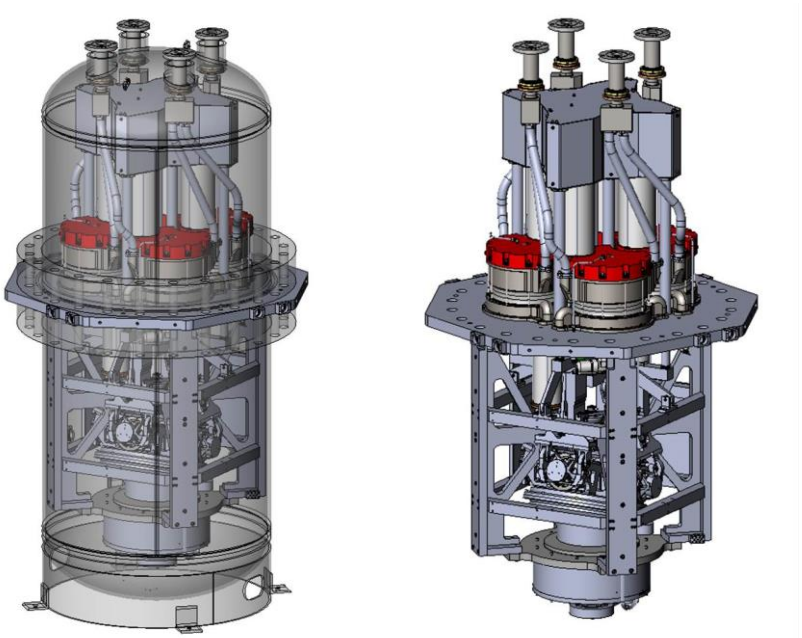

Figure 10. ThermoHeart Engine in pressure vessel (left); internal assembly (right).

Alternator: CEI chose what started out as an off-the-shelf, frameless, permanent-magnet alternator designed as a wind-turbine generator. The original power output rating of 31 kW_e at 600 rpm was de-rated to 26 kW_e at 650 rpm by the vendor, due to the addition of encapsulation material around the magnets by the vendor over their concern about operating the alternator in a pressurized nitrogen environment. CEI believes that the encapsulation material is not necessary, and future alternators will not have this feature. Because of the frameless construction, special handling and assembly methods are required, to make sure that the rotor, upon which the permanent magnets are bonded, does not crash into the stator due to the strong magnetic attraction between them. This is accomplished by bolting the stator and the rotor to a mounting flange at the factory, which holds the rotor in the correct relationship with the stator. When the alternator is installed in the engine, the stator is mounted to the engine frame and the rotor is mounted to the axle, and only then is the mounting flange removed. Figure 11 shows the alternator prior to installation.

Figure 11. Permanent magnet alternator prior to installation.

Instrumentation: An electronic encoder was installed on the main axle to give a precise, real-time position of the angular position of the axle, which is needed for calculating the instantaneous working volumes of each thermodynamic circuit. Thermocouples were installed on each of the eight diffusers, in the insulated volume above the hot pistons, in the un-insulated volume containing the mechanism and alternator, and on the alternator. Differential pressure transducers were installed between each of the four cold working volumes (the volume between a cold heat exchanger and its respective cold cylinder) and the interior of the pressure vessel. These pressure transducers measure the instantaneous pressure developed between the cold working volume and the interior of the pressure vessel. Additional differential pressure transducers were installed between each of the four hot working volumes (the volume between a hot heat exchanger and its respective hot cylinder) and their respective cold working volumes. These pressure transducers measure the difference between the instantaneous pressure in each hot working volume and that in its corresponding cold working volume, and thus measure the pressure drop of the gas as it flows through the hot and cold heat exchangers and the regenerator. In LabVIEW, the data acquisition software tool, this pressure drop is added to the cold working volume pressure to obtain the hot working volume pressure. Both are needed to accurately compute indicated power. Obtaining the hot working volume pressure this way results in a calculation of the indicated power that is more accurate than if this pressure were measured directly.

Outside of the pressure vessel, precision differential thermocouples were installed between the hot fluid inlet and outlet piping, and between the cold fluid inlet and outlet piping. A flow meter was installed in the hot heat transfer fluid piping, as well as the cold side plumbing. Pressure vessel gas charge pressure is monitored with another electronic pressure transducer. An electrical power meter is used to measure the instantaneous output voltage, current and flow direction, and power of the electricity consumed by (on start-up) or produced by (during power generation) the permanent-magnet alternator.

Data acquisition: A cRIO National Instruments data acquisition system, running under control of the LabVIEW data collection and instrument control software, gathers and processes the data taken by the above sensors. Near-real-time calculations include indicated power and thermal efficiency. A typical screenshot is shown in Figure 12 below.

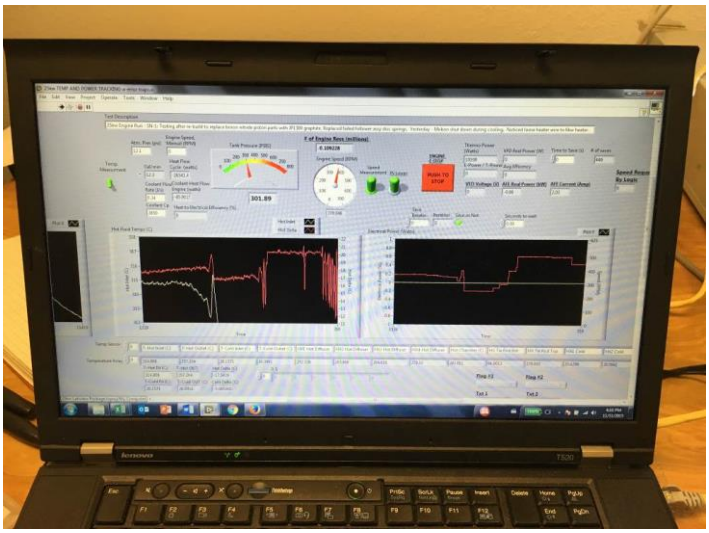

Figure 12. Data acquisition computer displaying real-time engine performance.

Starting system: Electrically actuated valves vent the thermodynamic working volumes to the interior of the pressure vessel during starting. This allows the engine to be spun up to a starting speed using a minimum of drive power while not developing pressure within the thermodynamic circuits. Once the desired start-up speed is achieved, the valves are closed, and the thermodynamic circuits begin to develop positive net power and drive the alternator.

Thermal insulation: The upper portion of the pressure vessel is insulated from the hot surfaces of the hot heat transfer fluid tubing, hot pistons, hot cylinders, hot heat exchangers, hot diffusers, and the regenerator canisters. Because the hot-side temperature is low enough for the hot-side pistons to safely contact their cylinders while sliding, the hot-side pistons and cylinders operate at the hot-side temperature. Thus, no insulating caps are used on the hot pistons, eliminating the pumping loss [7] and the shuttle conduction loss [7], [8]. Because the layout of the 25 kW ThermoHeart Engine has a clear demarcation between a single hot zone and a single cold zone, insulating the hot zone has been both more straightforward and more effective than on previous engines, as evidenced by the long time it takes for the hot zone to cool down when the engine is stopped. Figure 13 below shows the fully-insulated engine hot side assembly.

Figure 13. Insulated hot side of the 25 kW ThermoHeart Engine

Thermal fluid handling systems: The hot (heat supply) fluid circuit includes burst disks to protect the equipment upstream of the 25 kW ThermoHeart Engine from pressurization if high-pressure nitrogen gas breaches any pressure containment interface and flows into the fluid circuit. Provision has also been made to dissipate the low pressure but high volume flow rate of any leaked nitrogen at its discharge point to the atmosphere, and to contain any entrained hot heat transfer fluid in the nitrogen before the nitrogen is released to the atmosphere. The cold (heat rejection) fluid circuit consists of PVC manifolds and reinforced plastic tubing connecting the ThermoHeart Engine to a chiller or fan-coil heat-rejection unit.

Thermal test system: The hot-side heat transfer fluid is a high-temperature thermal oil heated in a natural-gas-fired oil heater. The cold-side heat transfer fluid is water cooled in a mechanical-refrigeration chiller. Figure 14 shows the 25 kW ThermoHeart Engine connected to the hot-side oil plumbing on top of the pressure vessel and to the cold-side water plumbing at the cold plate between the flanges of the pressure vessel.

Figure 14. The 25 kW ThermoHeart Engine connected to the hot and cold plumbing.

Control system: In anticipation of the advanced operating requirements of a planned field installation, an inverter and power conditioning and grid-tie electronics were incorporated into the controller, allowing electricity generated by the 25 kW ThermoHeart Engine to be fed onto the utility grid, rather than be wasted in an electrical resistance load. The inverter is used as the electronic load to regulate engine speed. Power flow in the system is bidirectional, enabling the controller to supply electric power to the 25 kW ThermoHeart Engine to start it. Current loading of the alternator and hence torque loading of the engine is achieved by a variable frequency drive (VFD) used as an active rectifier. Speed is set by either direct input via the front panel of the controller or by an automated computer controller via Ethernet. Sustainable Power Systems (SPS) was contracted to provide an engine controller, a stand-alone overspeed protection function, and electric power dump resistors to absorb the 25 kW ThermoHeart Engine's power in the event of an overspeed fault and subsequent shutdown. The overspeed protection function is an independent circuit in a separate cabinet connected directly to the engine's electric power feedthrough.

A second strategic partner, Schneider Electric, also designed a control system, consisting of the engine starter, controller, inverter, power conditioner, and grid tie, as part of a solar-thermal-powered Stirling generator project to supply electric power to micro-grid utilities. This controller interfaces to SPS's overspeed protection circuit and to the micro-grid.

Both controllers have been commissioned and have demonstrated correct operation in starting, speed-controlling, and stopping the engine. Both controllers implement overspeed shut-down procedures independently of the overspeed protection circuit. Both controllers automatically handle the switchover between electric power going into the 25 kW ThermoHeart Engine to start it and electric power produced by the engine when it is running. The important protocols for handling faults, alarms, and notification have been implemented in both controllers and the overspeed protection circuit.

The SPS controller is shown on the left in Figure 15 below, and the Schneider Electric controller is shown on the right.

Figure 15. Engine controller/inverter system provided by Sustainable Power Systems in operation (left) and the Schneider Electric system in operation (right).

1. THEORY/CALCULATIONS

Analysis, optimization, and design: Commercial software for multivariate generalized reduced gradient methods was used to optimize the thermodynamically significant details of the engine to arrive at design specifications (e.g., bore, stroke, heat exchanger dimensions, number of heat exchanger tubes, regenerator dimensions, regenerator wire dimensions and spacing or foil thickness and gap, number of regenerator screens or foil windings), subject to constraints (e.g. Reynolds numbers, maximum pressure developed within cylinders, manufacturing limitations, maximum allowed stresses). This optimization process was implemented within a proprietary engine design software tool developed at CEI, and optimization metrics have variously included efficiency, levelized cost of energy, and engine cost.

A rigid-body dynamic model of the linear-to-rotary mechanism, called the mechanism model, was developed to model all translational and rotational geometry, velocities, accelerations, and all forces and moments in the linear-to-rotary mechanism. The mechanism model was first used to specify and optimize the geometry of the 4-bar linkage, configured as a Watt linkage, to produce the linear-motion point on its center link having the nearly straight-line motion that is acceptably accurate to function as a crosshead where the piston rods and bails are attached, and thereby minimize side loads between the pistons and cylinders. Although the Watt linkage is capable of producing five collinear points within the range of the nearly straight-line motion, the solution chosen has only three, which allowed the links and the linear-motion point to be more conveniently located. Nonetheless, the deviation from perfect straight-line motion of the linear-motion point is less than + or - 0.31 mm over a stroke length of 168 mm, which is better than two parts in a thousand.

Outputs of the mechanism model, along with other criteria, were then used to set bounds on the cylinder bores of the expansion (hot) and compression (cold) spaces, the piston stroke, engine speed, and charge pressure.

The mechanism model executes ”describing functions” that calculate power output as a function of the hot-side and cold-side heat transfer fluid temperatures, engine speed, and charge pressure. These describing functions also calculate the instantaneous pressure within the working volumes as a function of angular position of the main axle. The describing

functions are extracted from results calculated by the proprietary engine design tool with Eureqa, a data-mining software tool for discovering mathematical relationships in data. The mechanism model calculates all forces and couples on all components, including gyroscopic couples and traction forces on the cam followers, the minimum force of preload springs necessary to prevent slippage between the cam followers and the cam, the harmonics of all unbalanced forces and couples that have to be reacted by the engine mounts, values of the terms in the inertia tensor of the main axle assembly necessary to cancel the first harmonic of all of these forces and couples, and the instantaneous kinetic energy of all moving parts. Correctness of the mechanism model was verified with Motion, the dynamic modeling tool in the SolidWorks CAD/FEA software, which can analyze but not optimize.

Each pivot or axle is supported by antifriction bearings. Load models were found in the literature or ball bearing manufacturers' engineering guides for five different types of antifriction bearings, and incorporated into the mechanism model. The instantaneous speed, radial force, and axial force calculated by the mechanism model are used in the load models to calculate the "equivalent load," a constant load under which a bearing would have the same lifetime as under the actual, time-varying load. The lifetime of each bearing, assumed to follow the 2-parameter Weibull probability distribution, was then calculated, from which the system lifetime was calculated. An optimal combination of the bearings' dynamic load ratings was found such that a penalty function, such as mass or cost, was minimized, subject to the constraint that the system achieve a specified lifetime with 90% probability. Bearings having dynamic load ratings closest to those calculated were selected from catalog offerings. The dynamic load ratings of these bearings were entered into the mechanism model, to confirm that the actual design meets or exceeds the lifetime specification. In a separate analysis, the 2-parameter Weibull probability distribution was also used to estimate the system lifetime of the four rolling interfaces between the cam and the four cam followers.

A representative output of the mechanism model is shown below in Figure 16, which shows a magnification of the deviation from straight line motion of the linear-motion point.

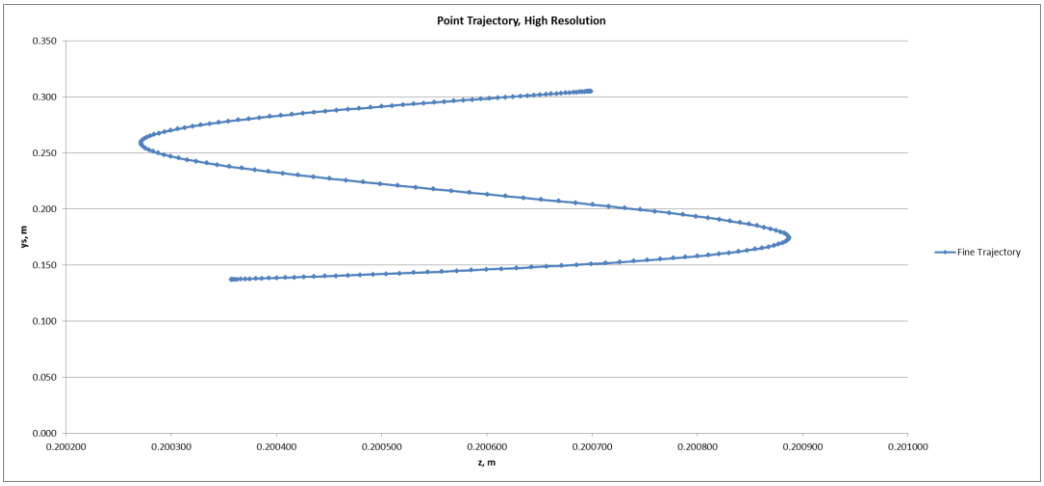

Figure 16. Representative output of the mechanism model.

Stress and fatigue life: Finite element analyses of stresses in internal components due to distortions from thermal expansion and from pressure and inertial forces were performed using modules within the SolidWorks CAD/FEA software. A design lifetime goal was set for each component that transmits force, ranging from 20,000 hours for piston rings and main bearings to 60,000 hours for the drive train.

The time-averaged torque output is very nearly proportional to the ratio of the hot-side temperature to the cold-side temperature (called the temperature ratio), and very nearly proportional to the charge pressure. For a given temperature ratio and charge pressure, there is an optimum speed that maximizes expected bearing lifetime. Operation at the optimum speed is called the "tuned condition." Figure 17 shows the effect on bearing lifetime of operating the engine off the tuned condition by varying the charge pressure, over a series of different speeds. The charge pressure is represented as the fraction of the optimum pressure that maximizes bearing lifetime at a given speed. Maximum lifetime for a given speed thus occurs when the fraction is 1.00. Lifetime is the number of operational hours the mechanism has a 90% chance of having no bearing failures.

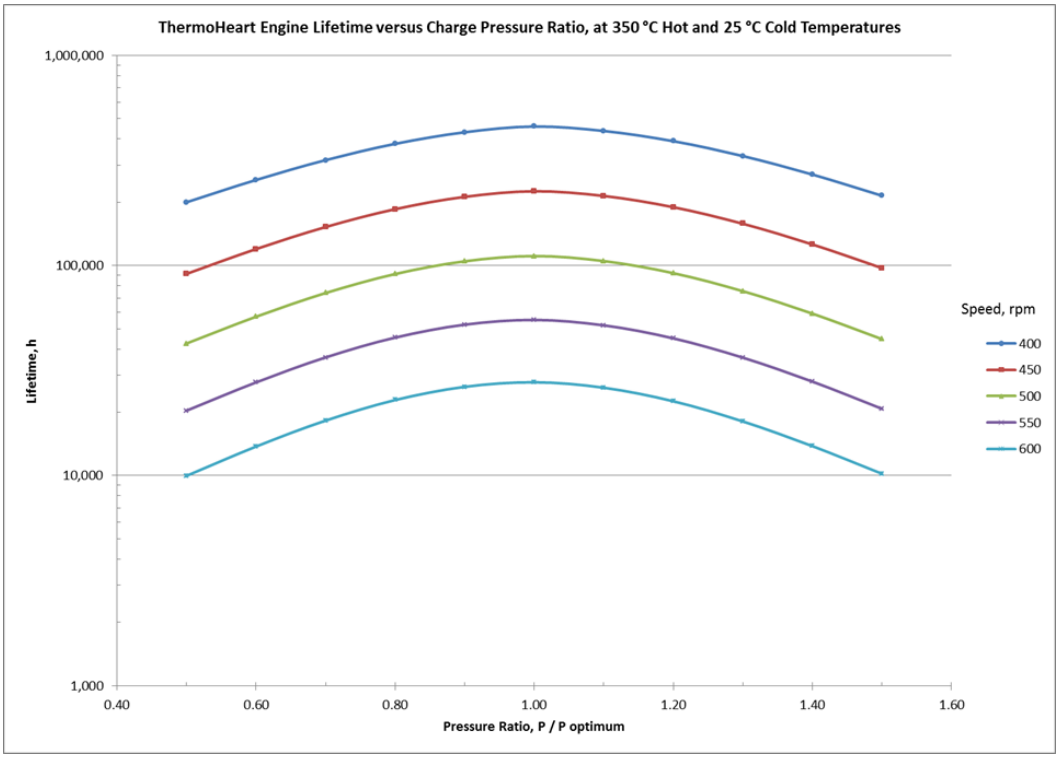

Figure 17. Impact of changing charge pressure on bearing lifetime, at different speeds.

2. RESULTS

The linear-to-rotary mechanism has now run under power-producing conditions for approximately 170 hours. Except at the highest speeds, there is minimal vibration and noise. The engine is quietest when the speed and pressure correspond to the tuned condition.

Initial Testing Results: Both the SPS and the second control systems have operated the 25 kW ThermoHeart Engine. Representative test results from April and May, 2016 are shown in Tables 2 and 3 below. In Table 2, the engine was operated at less than maximum power but near maximum efficiency. Power output is estimated to be between 52% and 55% of maximum. In Table 3, the engine was operated near maximum power for each test point.

Real-time pressure data is captured by the test system from the differential pressure transducers at every pulse of the electronic encoder attached to the main axle. The pressure data can be used with the instantaneous hot-side and cold-side working volumes calculated at every pulse to generate pressure-volume work loops, which can be compared to those calculated by the engine design software tool.

Table 2. Test results from April and May, 2016. Operation near maximum efficiency.

Hot-Side Temp, °C	Generator Gross Output Power, W	Thermal Input Power, W	Thermal-to-Electrical Efficiency
247	8842	35405	25.0%
272	10297	39679	26.0%
305	11911	43600	27.3%
341	13840	44675	31.0%

Table 3. Test results from April and May, 2016. Operation near maximum power.

Hot-Side Temp, °C	Generator Gross Output Power, W	Thermal Input Power, W	Thermal-to-Electrical Efficiency
218	11079	64408	17.2%
237	13058	66723	19.6%
249	14216	67933	20.9%
268	16351	71770	22.8%
281	17534	73746	23.8%

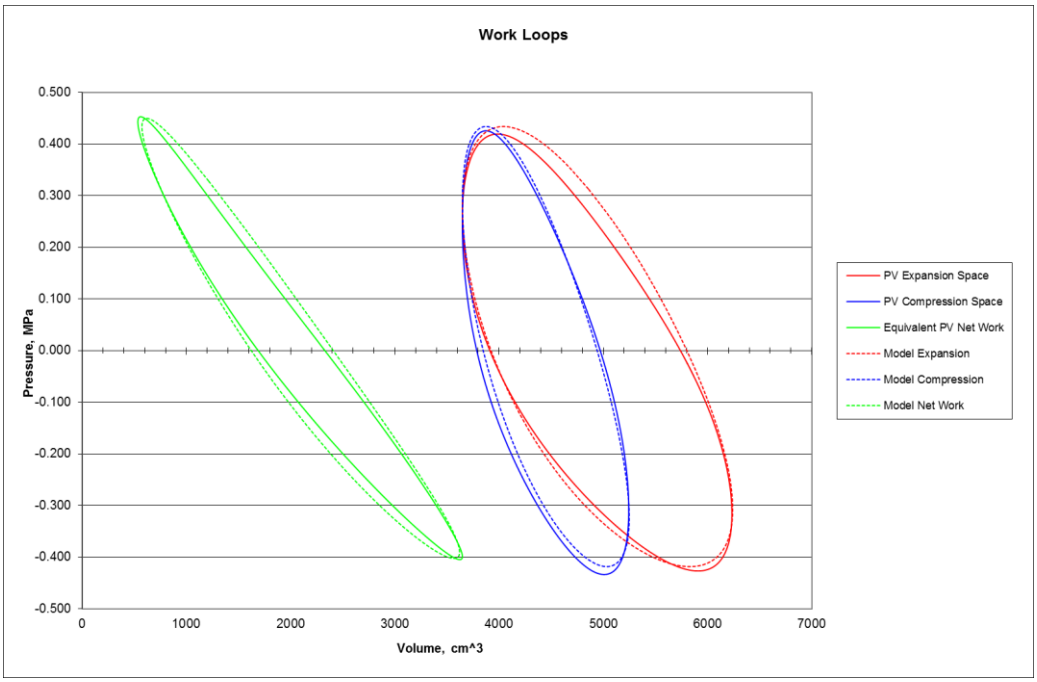

Figure 18. Overlay of measured and calculated work loops. Hot-side temperature is 270 °C, cold-side temperature is 22 °C, pressure is 2.86 MPa, and speed is 600 rpm.

In Figure 18 above, the measured expansion space (hot side), compression space (cold side), and net work loops are overlaid with the calculated ones. If the hot-side and cold-side pressures were identical, the net work loop could be calculated using a single pressure and adding the hot-side and cold-side working volumes to get a single working volume. Because of the pressure drop of the gas as it flows through the hot and cold heat exchangers and the regenerator, however, the hot-side and cold-side pressures are not identical. Hence, the net work loop is constructed by using the cold-side pressure for both working volumes, but, before adding the hot-side and cold-side working volumes, decrementing the hot-side working

volume by the fraction that the actual hot-side pressure is greater than the cold-side pressure. Detailed comparison of the work loops is given in Table 4 below.

Table 4. Measured versus Calculated Work Loop Comparison

	Measured	Calculated	Ratio
Expansion Work, J	1171	1242	0.943
Compression Work, J	-773	-749	1.032
Net Work, J	399	494	0.808
Indicated Efficiency (Net Work / Expansion Work)	0.340	0.397	0.856

3. DISCUSSION

Comparison of testing results with current technologies: Figure 20 below shows the published thermal efficiencies of various power generation systems from different suppliers, along with test results for CEI's 25 kW ThermoHeart Stirling engine.

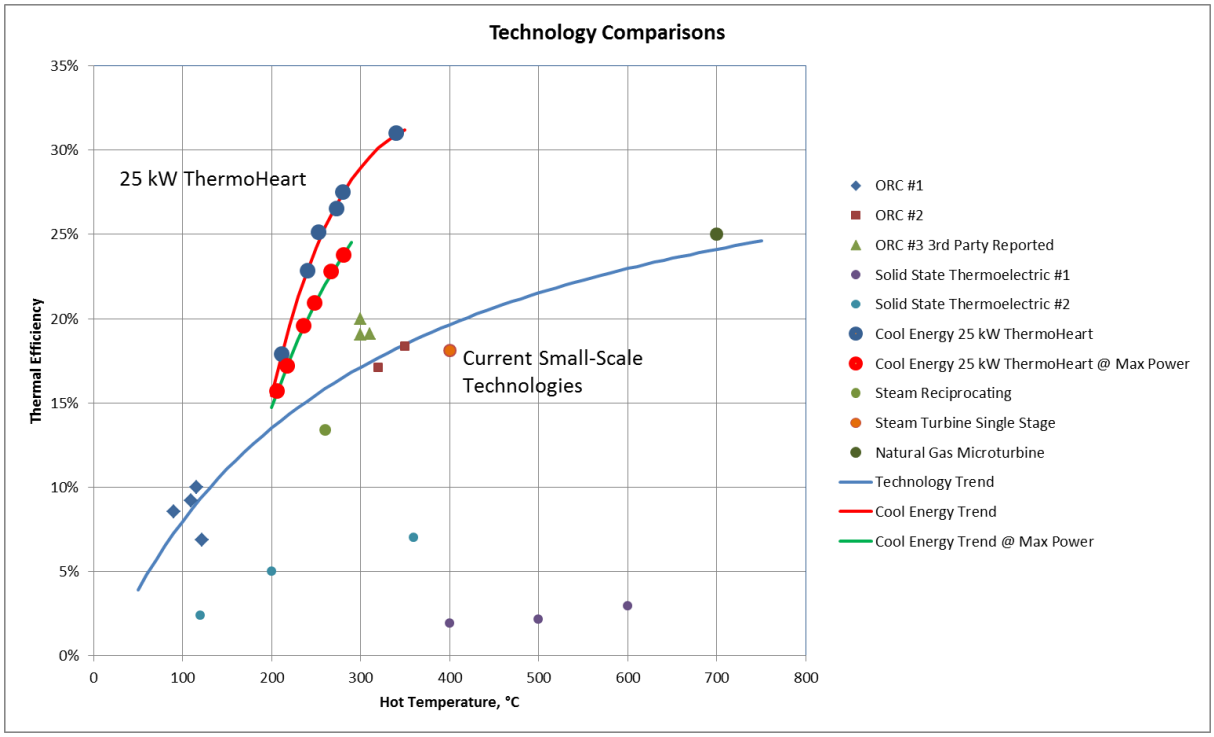

Figure 19. Stirling engine test results compared to reported results from other systems.

As shown in Figure 19, the gross thermal-to-electrical conversion efficiency measured for the Stirling engine is notably higher than any of the other small-scale technologies surveyed for comparable hot-side temperatures, for both maximum efficiency and maximum power operation. The Technology Trend line on the graph is a fit through the reported efficiencies of various small-scale Rankine-cycle and micro-turbine technologies. At the highest Stirling engine power output test condition represented by the green line on the chart, the peak measured thermal-to-electrical efficiency is 23.8%, which is 51.5% of the Carnot limit, and which compares to the Curzhon-Ahlborn (or Chambadal-Novikov) efficiency of 26.7% [9]. At highest efficiency test condition represented by the red line on the chart, the peak measured thermal-to-electrical efficiency is 31.0%, which is 60.2% of the Carnot limit, and just higher than the Curzhon-Ahlborn efficiency of 30.4%.

4. CONCLUSIONS

It has been demonstrated that a Stirling engine can be designed, optimized, and built that produces economically significant amounts of electric power from low-to-medium temperature heat sources. There are multiple applications for an engine of this type, including waste heat recovery, concentrating and non-concentrating solar thermal systems, biomass combustion or gasification, and power generation from liquefied natural gas evaporation.

5. ACKNOWLEDGEMENTS

Over the course of the development of this low-temperature engine architecture, funding support has been received from private investors, sales of engines, components, and services, and grant awards. Along with our partners and employees, Cool Energy would like to thank the National Science Foundation, the Environmental Protection Agency, the Department of Energy and the State of Colorado for grant support that has substantially advanced this work.

6. REFERENCES

[1] Chen NCJ, Griffin FP, West CD. Linear Harmonic Analysis for Stirling Machines and Second Law Analysis of Four Important Losses. CONF-840804—39, Proceedings of the 19th Intersociety Energy Conversion Engineering Conference, August 1984

[2] Chen NCJ, Griffin FP, West CD. Linear Harmonic Analysis of Stirling Engine Thermodynamics. ORNL/CON-155, Martin Marietta Energy Systems, Inc., Oak Ridge Nat'l. Lab., August 1984

[3] Span R, Lemmon EW, Jacobsen RT, Wagner W, Yokozeki A. A Reference Equation of State for the Thermodynamic Properties of Nitrogen for Temperatures from 63.151 to 1000 K and Pressures to 2200 MPa. J. Phys. Chem. Ref. Data (2000), 29:6

[4] Lemmon EW, Jacobsen RT. Viscosity and Thermal Conductivity Equations for Nitrogen, Oxygen, Argon, and Air. International Journal of Thermophysics (2004), 25:1

[5] Organ AJ. The Regenerator and the Stirling Engine. Mechanical Engineering Publications Limited, London and Bury St., Edmunds, UK 1997

[6] Ibrahim MB, Tew RC Jr. Stirling Convertor Regenerators. CRC Press, Taylor & Francis Group, Boca Raton 2012

[7] Tew RC Jr. Overview of Heat Transfer and Fluid Flow Problem Areas Encountered in Stirling Engine Modeling. Lewis Research Center (1988), NASA TM-100131

[8] Chang HM, Park DJ, Jeong S. Effect of gap flow on shuttle heat transfer. Cryogenics (2000), 40:159-166

[9] Curzon FL, Ahlborn B. Efficiency of a Carnot Engine at Maximum Power Output. Am. J. Phys. (1975), 43:22

7. NOMENCLATURE

CEI Cool Energy, Incorporated
NIST National Institute of Standards and Technology
SPS Sustainable Power Systems
VFD Variable Frequency Drive